NASA CR-72589
NOLTR 70-15

GAS OPACITY MEASUREMENTS WITH A BALLISTIC PISTON COMPRESSOR

by

G. T. Lalos and G. L. Hammond

prepared for

NATIONAL AERONAUTICS AND SPACE ADMINISTRATION

Interagency Number C-7757B

U.S. NAVAL ORDNANCE LABORATORY

NASA CR-72589
NOLTR 70-15

FINAL REPORT

GAS OPACITY MEASUREMENTS WITH A BALLISTIC PISTON COMPRESSOR

by

G. T. Lalos and G. L. Hammond

prepared for

NATIONAL AERONAUTICS AND SPACE ADMINISTRATION

November 21, 1969

Interagency Number C-7757B

Technical Management
NASA Lewis Research Center
Cleveland, Ohio
Nuclear Systems Division
R. W. Patch

NAVAL ORDNANCE LABORATORY
White Oak, Maryland

ABSTRACT

The NOL Ballistic Piston Compressor was modified for opacity measurements in the ultraviolet between 1750 and 2500 Å. Principal changes consisted of lengthening the compressor stroke to eight meters, use of a 4-port test section for simultaneous emission and absorption measurements, use of Suprasil and MgF_2 windows and lenses, installation of a high intensity flashlamp, and use of high purity carrier gases. Opacity calculations using the best available literature values of photoabsorption cross sections predicted measurable opacity ($\tau > 0.05$) at wavelengths shorter than 2000 Å for a 10% H_2/90% He gas mixture at P = 2000 atmospheres and T = 5000°K. Results of control shot experiments with pure helium and with pure argon revealed anomalously high ultraviolet opacity, and prevented the projected hydrogen opacity measurements. Possible causes of the anomalous opacity are discussed and further steps that may be taken to reduce the impurity level are proposed.

TABLE OF CONTENTS

Section		Page
	LIST OF ILLUSTRATIONS	iii
1.0	INTRODUCTION	1
2.0	HYDROGEN OPACITY.	2
	2.1 Opacity Mechanisms	2
	2.2 Equilibrium Concentrations	10
	2.3 Calculated Opacity	11
3.0	BALLISTIC PISTON COMPRESSOR EXPERIMENTS	12
	3.1 Apparatus and Basic Technique	12
	3.2 Experimental Techniques	15
	3.2.1 Temperature Measurements	15
	3.2.2 Emission Experiments.	19
	3.2.3 Absorption Experiments	20
4.0	EXPERIMENTAL RESULTS.	23
5.0	ANALYSIS	25
	5.1 Impurity Opacities.	25
	5.2 Estimates of Impurity Abundances.	26
6.0	DISCUSSION.	27
7.0	CONCLUSION.	28
	REFERENCES.	30
	FIGURES	31

ILLUSTRATIONS

Figure	Title	Page
1	Calculated Opacity of a 10% H_2/90% He Mixture for P = 2000 Atm, and T = 5000°K	31
2	Schematic Diagram of Ballistic Piston Compressor . .	32
3	High Pressure Test Section	33
4	Multiple-Pass Optics for Increased Detection Sensitivity.	34
5	Disassembled Rulon LD Double-Cup Piston Seals. . . .	35
6	Optical Bench Isolated from Compressor	36
7	Regular Gas-Handling System.	37
8	High Purity Gas-Handling System.	38
9	Optics for Temperature Measurements.	39
10	Spectroscopically Measured Temperature for Helium. Thermometric Species: C_2, Ca	40
11	Spectroscopically Measured Temperature for Helium. Thermometric Species: C_2, Ca, Cu, Na	41
12	Half-Section of Flashlamp Assembly	42
13	Flashlamp Capacitor Discharge Circuit.	43
14	Optics for Ultraviolet Opacity Measurements.	44
15	Flashlamp Air Absorption Spectrum Showing Absence of Scattered Light in Ultraviolet.	45

1.0 INTRODUCTION

There is an increasing need for quantitative measurements of the spectral opacity of hot, highly compressed gases and gas mixtures. Design and construction of high energy density power sources such as the gaseous core nuclear rocket engine require hydrogen spectral opacity information for minimizing heat transfer to the engine walls, and for further heating of the hydrogen gas before it exits the nozzle, whereas proper definition of the stellar atmospheres of white dwarfs depends on radiative heat transfer calculations based on accurate values of absorption coefficients of gases in the hot, highly compressed state.

The investigations described in this report represent a continuation of a study undertaken for NASA of the opacity mechanisms present in a hydrogen/helium plasma at a temperature of 5000°K, and a pressure of about 2000 atm* (Ref. 1). Special attention was paid to the ultraviolet spectral region 1750 to 2500 Å where quasi-molecular hydrogen association is expected to be an important opacity producing mechanism.

Inasmuch as the conventional static methods of gas containment are inadequate for the physical conditions of interest in this investigation, it was necessary to employ a Ballistic Piston Compressor (Ref. 2). This device utilizes a free, tight-fitting piston in a

---

*Present study was funded jointly by NASA and the independent research program of the Naval Ordnance Laboratory.

closed-end tube as the gas container. Firing the free piston toward the end-plug compresses the trapped gas along the isentrope defined by its initial pressure and temperature, and results in high simultaneous values of pressure and temperature for times of about one-half millisecond. Measurement of the parameters of interest is made during the peak pressure and temperature of the compression cycle. When working along the NTP isentrope, the low ratio of specific heats of hydrogen makes it necessary to compress to pressures considerably in excess of 2000 atm in order to attain the required 5000°K gas temperature, and, additionally, results in an end-plug/piston separation smaller than the minimum 1 cm separation necessary for opacity measurements. Using a hydrogen/helium mixture increases the specific heat ratio and circumvents these difficulties.

2.0 HYDROGEN OPACITY

2.1 Opacity Mechanisms

In a partially ionized hydrogen plasma characterized by a pressure of 2000 atm and a 5000°K temperature, excited states are not sufficiently populated to produce measurable discrete line (bound-bound) opacity in the 1750 to 2500 Å wavelength region. Several continuum producing mechanisms (bound-free, free-free), however, are reasonably strong in this wavelength region and show promise of experimental detection. In addition, Rayleigh and Thompson scattering will also contribute to the total observed opacity.

In order to determine the accuracy with which absorption coefficients must be measured to determine the opacity due to any one of these absorption processes, it is necessary to estimate from available theory the relative magnitudes of each absorption coefficient. It is also helpful to know the wavelength dependence of each absorption coefficient as an aid in the experimental identification of the principal absorption processes. Current knowledge of the continuous absorption coefficients being considered here ranges from experimental verification to within a few percent of theory for photodetachment of H^-, to considerable theoretical uncertainty and no experimental observations for quasi-molecular hydrogen absorption. The photoabsorption processes occurring in a partially ionized hydrogen plasma most likely to contribute significantly to the opacity in the 1750 to 2500 Å wavelength range are listed below. The headings of the various processes refer to the combined system taking part in the photoabsorption process, i.e., negative hydrogen ion (free-free) refers to neutral atom Bremsstrahlung. All absorption coefficient formulae given here are in cgs units.

Negative Hydrogen Ion

The absorption coefficient per neutral hydrogen atom due to the free-free reaction

$$H + e + h\nu \rightarrow H + e \qquad (1)$$

is given by the approximation formula (Ref. 4)

$$a_\nu(\lambda,\theta) = 10^{-26} p_e \{0.0053666 - 0.011493\,\theta + 0.027029\,\theta^2$$

$$- (3.2062 - 11.924\,\theta + 5.9390\,\theta^2)(\lambda/10^6)$$

$$- (0.40192 - 7.0355\,\theta + 0.34592\,\theta^2)(\lambda^2/10^9)\} \qquad (2)$$

where p_e is the electron pressure, θ is 5040/T and λ is the wavelength in angstroms. For the bound-free reaction

$$H^- + h\nu \rightarrow H + e \qquad (3)$$

the absorption coefficient is given by

$$a_\nu(\lambda,\theta) = 10^{-26} p_e (0.4158)\,\theta^{5/2}\, e^{1.726\,\theta}\,(1 - e^{-h\nu/kt})K^* \qquad (4)$$

For $14{,}200 \geq \lambda \geq 16{,}419$ Å

$$K^* = 0.269818\,\Lambda + 0.220190\,\Lambda^2 - 0.0411288\,\Lambda^3 + 0.00273236\,\Lambda^4 \qquad (5)$$

where $\Lambda = (16{,}419 - \lambda)/1000$,

and for $\lambda \leq 14{,}200$ Å

$$K^* = 0.00680133 + 0.178708\,\Lambda + 0.164790\,\Lambda^2$$

$$- 0.024842\,\Lambda^3 + 5.95244 \times 10^{-4}\,\Lambda^4 \qquad (6)$$

where now $\Lambda = \lambda/1000$. The bound-free absorption is zero for $\lambda > 16{,}419$ Å. Both equations include the effects of stimulated emission.

Atomic Hydrogen

The absorption coefficient is given by the sum of all

contributions of the bound-free reaction

$$H^* + h\nu \rightarrow H^+ + e \tag{7}$$

from states whose ionization energies are less than that of a photon of the frequency under consideration, plus absorption of the free-free reaction

$$H^+ + e + h\nu \rightarrow H^+ + e \tag{8}$$

Per neutral hydrogen atom the total absorption coefficient is (Ref. 4)

$$a_\nu = \frac{2.0898 \times 10^{-14} e^{-u_1}}{x^3 U_o(\theta, p_e)} (1-e^{-h\nu/kT}) \times \left\{ \sum_{m_o}^{m^*} g_{bf}(m,x) \frac{e^{u_m}}{m^3} + \frac{1}{2u_1}[e^{u_{m^*}} - 1 + g_{ff}(x,\theta)] \right\} \tag{9}$$

$u_m = (X/kT)/m^2$ where X is the ionization energy of hydrogen and m is the quantum number of the mth state, $x = 1/\lambda$ where λ is the wavelength in microns, U_o is the partition function for neutral H, m_o is the largest integer such that $u_m \leq h\nu/kT$, m* is the value of the highest bound state considered, typically 10 or 12, g_{bf} is the bound-free quantum-mechanical Gaunt factor and g_{ff} is the free-free quantum-mechanical Gaunt factor.

Negative Hydrogen Molecule

The absorption coefficient for the free-free reaction

$$H_2 + e + h\nu \rightarrow H_2 + e \qquad (10)$$

per H_2 molecule is given by (Ref. 4).

$$a_\nu(\lambda,\theta) = p_e 10^{-29}[(0.09319\ \theta + 2.857 - 0.9316/\theta)(\lambda/911.27)^2$$
$$- (2.600\ \theta + 6.831 - 4.933/\theta)(\lambda/911.27)$$
$$+ (35.29\ \theta - 9.804 - 10.62/\theta)$$
$$- (7452\ \theta - 62.48 + 0.4679/\theta)(911.27/\lambda)] \qquad (11)$$

Ionized Hydrogen Molecule

Emission coefficients (combined) tabulated as a function of wavelength and temperature (Ref. 5) are available for the bound-free reaction

$$H_2^+ (^2\Sigma_g^+) + h\nu \rightarrow (H + H^+)^2\Sigma_u^+ \qquad (12)$$

and for the free-free reaction

$$H + H^+ + h\nu \rightarrow H + H^+ \qquad (13)$$

These emission coefficients can be converted to absorption coefficients by use of Kirchoff's law.

Ionized Triatomic Hydrogen

Although there are considerable amounts of H_3^+ formed in relatively cool, high pressure plasmas (Ref. 6), there are no reliable estimates available for the absorption coefficients of this ion.

Quasi-Molecular Hydrogen

The ground state of molecular hydrogen is a singlet state. Ground state absorption

$$H_2(^1\Sigma_g^+) + h\nu \rightarrow H_2(^1\Sigma_u^+) \qquad (14)$$

occurs well below 1750 Å and is not of interest in this investigation. The ground state of the triplet state, formed by the collision of two hydrogen atoms with parallel electron spins, is located above the singlet ground state by an amount equal to the dissociation energy of hydrogen. Absorption by this free-bound process

$$H + H(^3\Sigma_u^+) + h\nu \rightarrow {}^3\Sigma_g^+ \qquad (15)$$

is continuous and falls within the wavelength region of 1750 - 2500 Å. Absorption cross sections for hydrogen quasi-molecular association have recently been refined, tabulated, and indeed proposed as an opacity source that may account for the anomalous absorption in the sun from about 4800 Å to shorter wavelengths (Ref. 7). There is no experimental confirmation of the calculated cross sections to date.

Rayleigh Scattering

The Rayleigh scattering cross section of H per neutral H atom in the ground state is (Ref. 4)

$$\sigma = 5.799 \times 10^{-13}/\lambda^4 + 1.422 \times 10^{-6}/\lambda^6 + 2.784/\lambda^8 \qquad (16)$$

where λ is in angstroms; this equation is not valid for $\lambda <$ Lyman-alpha. The analogous cross section for H_2 per H_2 molecule

is (Ref. 4)

$$\sigma = 8.14 \times 10^{-13}/\lambda^4 + 1.28 \times 10^{-6}/\lambda^6 + 1.61/\lambda^8 \qquad (17)$$

Thompson Scattering

Scattering by free electrons is independent of wavelength and is negligible for electron densities of interest in this investigation. The Thompson scattering cross section is (Ref. 4)

$$\sigma_t = 6.655 \times 10^{-25} \text{ cm}^2 \qquad (18)$$

When it is necessary to mix the hydrogen with helium, as it is in these experiments, there are several additional sources of opacity that should be considered.

Neutral Helium

Photoionization cross sections for the lower levels of helium are given by (Ref. 4)

$$a_\nu(\theta) = \sum_i k_\nu(i) \frac{g_i}{g_o} e^{-X/kT} \qquad (19)$$

where the summation is over all ionization edges whose threshold frequencies are less than that under consideration. Hydrogenic cross sections are used for the higher levels.

Negative Helium Ion

Inasmuch as the only bound state of He^- is about 19 ev above the ground state of He, its population will always be

negligible at the temperatures of interest in this study, and photodetachment of the He^- will not contribute significantly to the opacity. Free-free continuous absorption coefficients for the reaction

$$He + e + h\nu \rightarrow He + e \qquad (20)$$

are given in (Ref. 8).

Rayleigh Scattering

The He Rayleigh scattering cross section is taken to be 0.134 times that of atomic hydrogen (Ref. 9).

Red Wing of Lyman Alpha

Extreme pressure broadening of the Lyman alpha line might be expected to produce measurable opacity in the far red wing, i.e., between 1750 and 2500 Å. The dominant broadening mechanism for high atomic hydrogen densities at the temperatures of interest is resonance broadening. This process occurs when the upper or lower state of the spectral line has an allowed dipole transition to the ground state, and when the active atom is perturbed by an identical ground state atom. Unfortunately, the theory of resonance broadening of spectral lines by atom-atom impacts (Ref. 10) is valid only for binary collisions, i.e., for low atomic hydrogen particle densities, and is not applicable to the high particle densities of these experiments, i.e., $n_H \approx 10^{20}$ cm^{-3}. Recently, it has been pointed out (Ref. 11) that the conventional resonance broadening formula describing absorption in the wings of Lyman alpha seriously overestimates

the magnitude of the absorption at long wavelengths. These authors find that the absorption coefficient decreases exponentially with increasing wavelength above 1623 Å, and state that it is improbable that the resonance-broadened red wing is a significant source of opacity at wavelengths in excess of 2,000 Å. There are to date no experimental opacity measurements in this wavelength region ascribable to the red wing of Lyman alpha.

2.2 Equilibrium Concentrations

A computer program named PLASMA that determines chemical equilibrium in complex mixtures containing ionized as well as neutral species was updated to include recently acquired data on H_2^+ and H_3^+ (Ref. 3). This computational scheme, based on the minimization of the Gibbs free energy, calculates the equilibrium concentrations of product species of any arbitrary gas mixture as a function of pressure and temperature. Two variations of the basic scheme permit equilibrium composition calculations as a function of pressure and energy added to the system in the form of a chemical reaction or mechanical work performed by a piston compressing a gas, and also along an isentrope.

This program was used to determine the compressor firing conditions that would optimize the atomic hydrogen particle density. This is equivalent to optimizing the opacity because the two processes that make the largest contributions to the opacity, i.e., quasi-H_2 and H^-(bf,ff), both depend on the particle density of atomic hydrogen. Peak pressures of 2000 atm (approximate upper limit of side

window operation) and peak temperatures of 5000°K (approximate upper limit for chromium plating of test section) were assumed. Although pure H_2 compressed to these peak conditions would produce the highest opacity, the computer results showed that it is necessary to use a mixture of about 10% H_2 and 90% He (by volume) to assure that the minimum piston/end-plug separation does not fall below the 1 cm necessary for absorption measurements.

Computer results for the equilibrium concentrations, in units of cm^{-3}, of the product species of a 10% H_2/90% He plasma at 2000 atm and 5000°K are shown in Table 1.

Table 1. Equilibrium Concentrations

H_2	(2.29×10^{20})	H_3^+	(1.41×10^{14})
H	(1.17×10^{20})	e^-	(1.34×10^{14})
H^+	(1.18×10^{13})	H^-	(2.27×10^{13})
H_2^+	(6.12×10^{12})	He	(2.59×10^{21})

2.3 Calculated Opacity

The opacities, τ_i, of all the continuum photoabsorption processes described in Section 2.1 were computed for the particle densities of Table 1 and for a pathlength of 5 cm (diameter of test section). The results for all processes with $\tau_i > 10^{-5}$ and the sum $T = \sum_i \tau_i$ were plotted as a function of wavelength for the range 1750 to 2500 Å, Figure 1. A dashed horizontal line representing the experimental detection limit of five percent for single-pass measurement is also shown. Multiple-pass operation is expected to lower the limit of

detection further.

Examination of Fig. 1 reveals that quasi-H_2 is the dominant absorbing process throughout the entire wavelength region, increasing in strength with decreasing wavelength. Except for H^- (bf, ff) each of the other opacity sources contribute less than 10^{-3} to the total opacity. Opacity detection through test beam attenuation measurements should be possible for $\lambda < 2000$ Å. In view of the absence of any identifying features in the different individual curves it is fortunate that one of the processes (quasi-H_2) is clearly much stronger than the rest, and that it has a reasonably strong wavelength dependence. Experimental detection of gas opacity at wavelengths less than 2000 Å, and with this wavelength dependence, could safely be ascribed to the hydrogen quasi-molecular association process if our neglect of contributions from the Lyman-alpha red wing is indeed justified.

3.0 BALLISTIC PISTON COMPRESSOR EXPERIMENTS

3.1 Apparatus and Basic Technique

The Ballistic Piston Compressor used in this investigation is shown in Fig. 2. It is the same apparatus employed in the earlier study (Ref. 1) except that the former 4-meter tube was replaced by a two-section, 8-meter tube to facilitate absorption measurements at high volumetric compression ratios, and a new high pressure test section containing two pairs of diametrically opposite windows for

simultaneous absorption and emission experiments, and for multiple-pass test beam attenuation measurements, Fig. 3, has replaced the old test section. The use of the 4-window test section makes it possible to increase the detection sensitivity of the opacity measurements through double-pass and quadruple-pass operation as shown schematically in Fig. 4. The test beam can be either collimated or slightly divergent. An alternate arrangement of the optics for quadruple-pass operation is the replacement of the half-silvered mirror (M_4) by a fully silvered mirror containing a small hole, and employing a slightly diverging test beam.

All surfaces of the new test section exposed to hot gas were electroplated with 0.001 to 0.002 inches of chromium to suppress vaporization of the steel parts and the accompanying appearance of the rich iron spectrum. In addition, a new steel piston long enough that the rear seals do not cross the junction between the tube and test section, and with interchangeable bearings (piston rings) was designed and constructed. This change was made so that the effect of different bearing materials on the absorption and emission spectrum of the test gas could be investigated. Past experience has shown that a small amount of bearing material dust is invariably formed during each compressor firing. Spectrograms of intermediate and high temperature shots always contain the characteristic discrete-line spectrum of the bearing material, and may also contain contributions to the continuous spectrum. The ability to change bearing materials was expected to facilitate analysis of the continuum spectrum recorded in the hydrogen/helium experiments. A new piston

cup-seal material, Rulon LD, was tested with the steel piston. Rulon LD is basically Teflon, but has a 1000-fold increase in wear resistance over Teflon, lower deformation under load, greater stiffness and higher compressive strength. These new seals have operated without rupture or other failure up to 2000 atm maximum pressure. Fig. 5 shows a disassembled view of the double-cup Rulon LD piston seal.

Two gas handling systems were designed. One system, Fig. 6, is made up of 1/4-inch copper tubing and Viton-A O-ring sealed "Circle Seal" plug valves. This system was used for test shots or preliminary experiments for which ultrahigh purity test gas was not required. The other system, Fig. 7, is the high purity, tube pumping and filling system which was used for data-taking spectroscopic experiments. It incorporates a moderately large capacity vacuum pump, stainless steel tubing and ball valves, and a multiport connection to the compressor tube at a point just forward of the initial piston position. This high purity system is capable of attaining 10^{-4} torr vacuum, but five microns was the best attained in the tube due to leaks in the test section-tube-piston release section system. Sintered bronze filters were placed in all input lines to remove particles larger than ten microns. The tube and all parts of the piston and test section were washed with C.P. Acetone using Kimwipe swabs. This procedure was followed before each shot. Tube filling was accomplished by pumping down to five to ten microns, filling to about 800 torr and bleeding down to 760 torr.

All measuring optics are mounted independently from the compressor supports in order to eliminate any possibility of noise or optical misalignment that might be caused by compressor recoil motion or vibration. Fig. 8 is a photograph showing the optical bench used to isolate the various optical elements from the compressor. The high pressure test section (with two observation windows), carbon arc, rotating drum, McPherson 216 and B and L quartz spectrographs, and high-intensity flashlamp (see Section 3.2) are also visible.

3.2 Experimental Techniques

3.2.1 Temperature Measurements

A spectroscopic temperature measurement scheme has been developed, installed, and tested with pure helium test gas. These tests have been conducted over a range of gas pressures from 900 to 2000 atm, and have yielded measured gas temperatures ranging from 2500 to 5000°K. The scheme will be described in detail in a separate report (Ref. 12), but its principal features and results are described here.

The scheme employed is the "brightness-emissivity" method which is based on the solution of the radiative transfer equation for a homogeneous gas sample in local thermodynamic equilibrium (LTE). The intensity and opacity at the center of a spectral feature are simultaneously measured, and with a suitable calibration of the intensity measuring optics, the excitation temperature of the thermometric specie radiating the spectral feature can be calculated. Thermometric

species used to date include both metallic impurity vapors of sodium, calcium, and copper, and trace quantities of premixed methane in helium. In the latter case, the formation of C_2 radicals from the decomposition of CH_4 has permitted excitation temperatures for the C_2 (Swan) bands to be obtained under conditions of homogeneity and freedom from boundary layer problems.

The application of this scheme to the Ballistic Piston Compressor was found to be straightforward. The opacity is measured by passing a carbon arc light beam through the hot gas and into a spectrograph instrumented as a photoelectric polychromator. A diagram of the optics used is shown in Fig. 9. The use of the rotary chopper permits a separation of the detected signal into that part due to the attenuated carbon arc beam and that due to the emission from the hot gas. The optical depth at each wavelength channel is obtained from Lambert-Beer's law calculations. This part of the scheme is identical in principle and in application to the scheme described in some detail in Ref. 1.

The intensity measurements are obtained from that part of the detected signal obtained when the chopper has blocked the carbon arc beam. The optics are calibrated by passing light from a standard light source of known spectral radiance through the same optical path as that traversed by the light from the compressed hot gas. Care must be taken to ensure that all lenses and apertures are filled by both light sources. The standard source used is the Mole-Richardson Company Pyrometric Molarc Lamp, Type 2371, and its radiance has been accurately measured at NBS (Ref. 13).

The temperatures derived from these measurements are obtained from the following equation, which is written as a ratio of two equations. The numerators are the radiative transfer terms for the gas emission and absorption, and the denominators are the calibration terms for the carbon arc.

$$\frac{I_\lambda(g)}{I_\lambda(a)} = \frac{B_\lambda(T_g)[1-\exp(-\tau_\lambda)]}{B_\lambda(T_a)} \qquad (21)$$

$I_\lambda(g)$ and τ_λ are the gas emission signal and the optical depth at the wavelength λ corresponding to the peak of the broadened spectral line. $I_\lambda(a)$ and $B_\lambda(T_a)$ are the calibration signal and radiance of the carbon arc at temperature T_a and at the same λ as the emission and opacity measurements. Therefore, this equation can be solved directly for the gas temperature T_g, by using the explicit form for the Planck function $B_\lambda(T_g)$, because all the other terms have been directly measured.

Temperature measurements have been made to date on the resonance lines of sodium and calcium, on both a resonance line and a line with an excited lower state of copper, the (0,0) band-head of the C_2 Swan bands, and at several wavelengths in the continuum. Many experiments have been made in which temperature measurements were obtained simultaneously for more than one of the above species. No serious disagreements were detected for temperatures of any of these species with the exception of continuum temperatures which were almost always several hundred degrees cooler than the metallic or molecular species.

The measured gas temperature versus time history for four 1800 atm P_{max} shots for helium with 60 ppm CH_4 is shown in Fig. 10. Simultaneous C_2 and Ca observations were made during each shot for approximately one millisecond before and after P_{max} occurred. Although there is some discrepancy between the temperatures measured by the two thermometric species on the compression stroke, both species give identical temperatures at P_{max} and throughout the expansion stroke. Fig. 11 shows the relationship between measured T_{max} and measured P_{max} for shots made with the old 4-meter and the new 8-meter compressor employing C_2, CuI(5105 Å), CaI(4226 Å), and Na(D-lines) as the thermometric species. For most shots T_{max} lags P_{max} by about 200 microseconds. The lag is attributable to gas leakage across the piston during the peak of the compression cycle. The gas temperature at P_{max} is systematically less than T_{max} by about 100°K for P_{max} < 1600 atm for all thermometric species, but for P_{max} > 1600 atm metallic resonance line temperatures never exceed 4500°K. Temperatures greater than 4500°K can only be obtained from C_2 or excited Cu lines. The empirical power law:

$$\log_{10}\left(\frac{T}{T_o}\right) = (0.364 \pm 0.010) \log_{10}\left(\frac{P}{P_o}\right) \qquad (22)$$

describes the T, P data quite accurately, for T_o = 298°K, and P_o = 1 atm.

No direct tests of the homogeneity of the thermometric species in the test gas have been devised. Both the C_2 molecules and the excited Cu atoms are formed predominantly in the hot, central core

The measured gas temperature versus time history for four 1800 atm P_{max} shots for helium with 60 ppm CH_4 is shown in Fig. 10. Simultaneous C_2 and Ca observations were made during each shot for approximately one millisecond before and after P_{max} occurred. Although there is some discrepancy between the temperatures measured by the two thermometric species on the compression stroke, both species give identical temperatures at P_{max} and throughout the expansion stroke. Fig. 11 shows the relationship between measured T_{max} and measured P_{max} for shots made with the old 4-meter and the new 8-meter compressor employing C_2, CuI(5105 Å), CaI(4226 Å), and Na(D-lines) as the thermometric species. For most shots T_{max} lags P_{max} by about 200 microseconds. The lag is attributable to gas leakage across the piston during the peak of the compression cycle. The gas temperature at P_{max} is systematically less than T_{max} by about 100°K for P_{max} < 1600 atm for all thermometric species, but for P_{max} > 1600 atm metallic resonance line temperatures never exceed 4500°K. Temperatures greater than 4500°K can only be obtained from C_2 or excited Cu lines. The empirical power law:

$$\log_{10}\left(\frac{T}{T_o}\right) = (0.364 \pm 0.010) \log_{10}\left(\frac{P}{P_o}\right) \qquad (22)$$

describes the T, P data quite accurately, for T_o = 298°K, and P_o = 1 atm.

No direct tests of the homogeneity of the thermometric species in the test gas have been devised. Both the C_2 molecules and the excited Cu atoms are formed predominantly in the hot, central core

of the test gas, and both species yield higher temperatures than the metallic resonance line data which are subject to boundary layer absorption effects.

The existence of LTE can be inferred from excitation temperature agreement obtained from thermometric species expected to have widely differing values of excitation cross-sections for collisions with helium atoms. Although electrons are efficient collisional excitation partners, their abundance is thought to be less than the value required to establish excitation equilibrium. Until more definitive experiments can be conducted to establish the degree of LTE achieved, we assume that these excitation temperatures correspond to the translational temperatures of the helium atoms.

3.2.2 Emission Experiments

Survey emission spectra were made during most flashlamp absorption experiments by focusing the light beam emerging from the top window of the test section onto the slit of a Bausch and Lomb medium quartz prism spectrograph, Fig. 12. This spectrograph was loaded with Kodak I-F and 103-F plates which are sensitive to light in the wavelength range 2000 to 7000 Å. The sensitivity of the optics-spectrograph-plate combination falls off quite rapidly below 2500 Å due to absorption by air and emulsion gelatin.

All of the emission spectra recorded in these experiments revealed the usual collection of broadened metallic lines superimposed on a continuum whose intensity variations with wavelength were described in the last NASA report. No significant difference

in exposure levels was observed between He, Ar, and research grade Ar. It was noted, however, that the continuum intensity of these experiments was markedly weaker than that of the experiments described in the first report. This is undoubtedly a result of the use of the new test section with its newly chromium-plated bore, and the adoption of more stringent cleaning procedures for the compressor prior to each shot.

3.2.3 Absorption Experiments

In order to make opacity measurements in the ultraviolet it is necessary to use a lamp of high brightness temperature. A Garton-Charatis flashlamp with a 48,000°K brightness temperature was chosen, Fig. 12. The emitting medium of this lamp is a plasma consisting of hydrocarbons ablated from the phenolic capillary walls by the sliding-spark discharge, together with 5 mm Hg air representing the lamp firing pressure. The capillary dimensions are 3/16 inch diameter by 2-1/2 inch length, and the electrodes are of tungsten. During this investigation the flashlamp was operated at five kilovolts resulting in an input energy of 150 joules, peak measured current of 2500 amps, peak current density of 1.4 kiloamps/cm^2, and a visible brightness temperature of 30,000°K, a value obtained by extrapolation of the Charatis calibration data. The circuit diagram for the flashlamp is shown if Fig. 13. Oscilloscope display of the flashlamp intensity-time signal from a photomultiplier tube showed a fast rise to peak intensity in approximately 5 μsec followed by an exponential decay resulting in a pulse half-width of 10 μsec. I_{max} was reproducible to ± 3 percent.

The optical train (Fig. 14) traversed by the light pulse generated by the flashlamp plasma consists of a 6 mm thick Suprasil II flashlamp window, a 1 mm thick Suprasil disk aluminized to 35 percent transmission at 1900 Å, a 150 mm focal length (Lyman α) f/6 MgF_2 lens, two 12.27 mm Suprasil II high-pressure windows, a 45° angle of incidence front aluminized mirror, a 50 mm focal length f/2 MgF_2 lens, and a McPherson Model 216 combination monochromator-spectrograph-direct reader. The McPherson 216 has a Czerny-Turner mount and its 600 groove/mm, 2000 Å blazed B and L grating gives a 15.9 Å/mm reciprocal dispersion at 1900 Å. Adjustable entrance and exit slits set at 50 μ width produce a triangular slit function with a 0.8 Å half-width. The detector was a RCA 7200 photomultiplier tube with the cathode at -1000 volts. This tube is essentially a 1P21 in a Suprasil envelope giving S19 spectral sensitivity response. The RCA 7200 output was connected to a two-stage emitter-follower preamplifier and displayed on a Tektronix RM35 oxcilloscope.

The test beam signal and its attenuation were measured with two firings of the flashlamp. In order to be certain that I_o is the same for the two measurements a flashlamp monitor scheme was assembled, Fig. 14. The beam emerging from the front window of the flashlamp is split by the 1 mm thick Suprasil disk aluminized to 35 percent transmission at 1900 Å. The reflected beam passes through a Thin Film Products interference filter with a 200 Å bandpass centered at 2300 Å, a sodium salicylate coated (front surface) glass plate, and a four-foot section of fiber optics light guide to a RCA 6199 (S-11 response) photomultiplier/emitter-follower/oscilloscope display. This monitor

is sensitive enough to detect a one percent change in lamp intensity.

In order to determine the UV-cutoff of the optical train and its six meters of air, the flashlamp was flashed 30 times and recorded on Kodak SWR film using a 20 μ spectrograph (McPherson 216) slit. A Calcomp plot of the resulting spectrogram is shown in Fig. 15. Although absorption by the Schumann-Runge bands of O_2 starts at about 1950 Å and increases with decreasing wavelength, there are many wavelength intervals of very weak absorption between 1950 and 1875 Å. Below 1875 Å, strong apparatus/air absorption sets in. These "windows", located just to the blue of the red-degraded vibration-rotation bandheads, can be used for opacity measurements without recourse to vacuum operation. Removal of the air from the path of the test beam would extend the usable wavelength range to about 1750 Å where the MgF_2 and Suprasil optical elements begin to absorb strongly.

In spite of the extremely heavy exposure (blackening) on SWR film, there was no detectable blackening at the stronger O_2 Schumann-Runge bandheads, nor in many of the individual rotational lines. One can therefore conclude that scattered light makes a negligible contribution to the total intensity or signal at these wavelengths.

Estimates of random and systematic errors in individual measurements indicate an overall accuracy of the final opacity value of ± 4 percent. This value represents the sum of oscilloscope record reading (± 2%), flashlamp reproducibility, corrected with monitor

adjustment if necessary (± 1%), thermal effects such as spectrograph wavelength shifts, oscilloscope sensitivity drifts, and effects due to relative humidity changes in room (± 1%). Errors due to scattered light, optical alignment during shot, and defocusing at spectrograph slit due to refractivity changes in the test gas at high temperatures and pressures are negligible.

4.0 EXPERIMENTAL RESULTS

The initial conditions of the test gas for most of the experiments of this investigation were 1 atm pressure and room temperature. Eighteen compressor shots were made for UV opacity measurements at pressures up to 1850 atm and temperatures up to 4700°K. In addition, 45 temperature measurement shots were made at pressures up to 2480 atm and temperatures up to 5100°K.

A number of pure helium control shots with P = 1500 atm and T = 4000°K were made to check out all systems and to establish impurity radiation levels that would be used to correct measured radiation levels in the projected 2000 atm, 5000°K hydrogen/helium data shots. The initial results at a number of wavelengths between 1800 Å and 1900 Å revealed totally unexpected high values of the opacity, τ, ranging from 0.6 to 1.5. The opacity that can be ascribed to helium at these pressures and temperatures is less than the calculated 2000 atm, 5000°K value of 0.0015 (Fig. 1), and well below the detection limit of the measuring scheme. The observed opacity must therefore be due to impurities. Improved tube cleaning and filling techniques

were adopted and the experiments were repeated. The most reliable data (using the beam-splitter flashlamp monitor) were obtained at 1900 Å and showed a marked reduction in the data scatter from the initial measurements, but unfortunately still gave an unaccountably high opacity of $\tau = 1.08 \pm 0.07$. Air Products and Chemicals, Inc. 99.975 percent pure helium (principal impurities N_2, H_2O) was used for the driver gas, and 99.995 percent pure helium (50 ppm Ne, trace N_2) was used as the test gas. Tube pumping and filling procedures added approximately 50 ppm air to the test gas.

In order to eliminate any possibility that the observed control shot opacity was associated in some unknown way with the helium, it was decided to repeat the control shots but with argon instead of helium. The first argon shot was made with 99.97 percent pure argon (150 ppm H_2O, 150 ppm N_2) for both the test and driver gas and gave $\tau > 3.3$. The second and third argon shots were made with Linde Research Grade 99.999 percent pure argon (< 5 ppm He, 3 ppm N_2, trace Ne, H_2O) as the test gas. Tube pumping and filling resulted in the addition of approximately 60 ppm air to the test gas in the second shot giving $\tau = 1.55$, and 25 ppm helium and 20 ppm air in the third shot giving $\tau = 1.13$.

The essentially identical opacity measured in the helium and argon shots, i.e., 1.08 and 1.13 respectively, indicates that the unknown opacity source probably is not associated with the rare test gas, but is a common impurity introduced into the compressor with the test gases, or boiled off the test section walls in a similar fashion in both the pure helium and argon shots.

5.0 ANALYSIS

5.1 Impurity Opacities

Inasmuch as the observed ultraviolet continuum opacity cannot be ascribed to the test gases helium and argon it becomes necessary to look for other opacity producing mechanisms. One possible source of the observed opacity may be the ever-present trace amount of vapors of the metallic impurities, i.e., Na, Ca, K, Rb, Cs, Cu, Cr, and Fe that are unavoidably produced during the mechanical operation of the compressor. Photoionization of those metal vapor impurities with appropriate ionization potential could account for the observed ultraviolet continuum opacity.

Residual air in the tube from the test gas filling operation is an additional source of impurities. Pressure-broadened vibration-rotation lines of the Schumann-Runge ($B^3\Sigma \rightarrow X^3\Sigma$) system of O_2, and of the Lyman-Birge-Hopfield ($a^1\Pi_g \rightarrow X^1\Sigma^+_g$) and Vegard-Kaplan ($A^3\Sigma \rightarrow X^1\Sigma$) systems of N_2 may conceivably account for the observed opacity.

Analogous arguments hold also for the photodetachment continua associated with the minute amounts of O_2^-, N_2^-, OH^-, and Cu^- that can be expected to be present in the test gas at the peak of the compression cycle.

A final constituent of the hot, highly compressed test gas that may contribute to the test beam attenuation is particulate matter. A small amount of very fine dust is produced by the rubbing motion of

the phosphor-bronze piston rings on the polished steel walls of the tube during each compressor shot. It is possible that imperfect sealing of the reservoir gas by the Rulon cup-seals during the initial part of the compression cycle, when the reservoir driver gas pressure is greater than the test gas pressure, results in a small amount of dust being blown across the piston and mixed with the test gas.

5.2 Estimates of Impurity Abundances

Previous calculations (Ref. 1) based on experimental measurements of the opacity at the peak of the 4226.7 Å calcium line and the sodium D lines give abundances of these two impurities of approximately 10^{12} cm^{-3}. This value is probably a reasonably good estimate of the abundance for each of the metal vapor impurities. Fifty ppm residual air in the compressor tube from the filling operation represents abundances at the roughly 115 amagat peak relative density of these experiments of 1.2×10^{17} cm^{-3} for N_2 and 3.2×10^{16} cm^{-3} for O_2. The free electron abundance of $\approx 10^{13}$ cm^{-3} in the helium experiments is at most doubled by contributions from impurity ionization.

Estimates of the size and number density of the particulate impurity cannot be made easily. Visual inspection of the test section immediately after a compressor shot reveals a very thin layer of fine, reddish dust particles, which probably come from the phosphor-bronze piston rings.

6.0 DISCUSSION

Calculation of absorption coefficients of all possible photoabsorption processes involving helium, argon, and the above described vaporized impurities were made but the sum of the individual contributions was much less than the value of 0.2 cm^{-1} required to explain the experimentally measured opacity.

Attenuation of a test beam by particulate matter is due to both scattering and absorption processes. The scattering and absorption coefficients of particles ranging in size up to about 0.1 of the wavelength of the incident radiation increases quite rapidly with decreasing wavelength, whereas test beam attenuation by larger particles results in less severe frequency dependence. One can reason that scattering and absorption by particles of dimensions much less than the 1900 Å wavelength of the incident radiation produces the observed opacity. Unfortunately, this does not appear possible because the exceedingly small cross sections associated with these processes require an unrealistically high abundance of particulate matter.

The inability to ascribe the source of the measured opacity to known photoabsorption processes involving the high temperature product species of the carrier gas and known impurities makes it necessary to consider less likely processes previously neglected. Various hypothetical processes can be described even though insufficient data prevents meaningful evaluation. Photoabsorption

processes involving previously unobserved high-temperature, high-pressure species may be occurring. These species might include the dimer of helium, He_2, molecules HeX where X is an impurity, or some heretofore undetected impurity whose spectrum lies in the ultraviolet.

It may be argued that the ultraviolet transmissivity of the high-pressure windows is somehow degraded by the severe mechanical and thermal stresses occurring at the peak of the compression cycle. Mechanical stress is known not to be detrimental to the Suprasil window material in the visible, and it seems likely that the same also holds true for the ultraviolet. It is, however, conceivable that the inside window surface that is momentarily exposed to the 5000°K gas experiences thermal stresses that degrade its ultraviolet transmission properties. There are no measurements that suggest this as a possible mechanism, although in principle it is a remote possibility.

7.0 CONCLUSION

The actual data-taking H_2/H_e experiments must necessarily be postponed until the unexplained ultraviolet opacity source at 1900 Å is identified and removed. Further steps that may be taken include reducing the impurity level by simultaneous tube heating and pumping, chrome-plating the compressor tube, acid cleaning all parts exposed to hot gas, improving piston cup-seals so that less particulate matter is blown into and mixed with the test gas by the driver gas,

testing of alternate window materials in order to examine the possible effect of high temperature on window transmissivity, and studying the temperature and wavelength dependence of the observed opacity for any clues that may help identify its source.

REFERENCES

1. Lalos, G. T. and Hammond, G. L., 1966, NASA CR-72116.

2. Lalos, G. T. and Hammond, G. L., 1965, Rev. Sci. Instr. 36, 550.

3. Patch, R. and McBride, B., 1968, NASA TN D-4523.

4. Mihalas, D., 1967, "Methods of Computational Physics," Vol. 7, ed. B. Alder, Academic Press, N. Y. (Chapter 1).

5. Drawin, H. and Felenbok, P., 1965, "Data for Plasmas in Local Thermodynamic Equilibrium," Gauthier-Villars, Paris.

6. Patch, R., 1969, NASA TN D-4993, also JQSRT 9, 63.

7. Doyle, R., 1968, Ap. J. 153, 987.

8. Somerville, W., 1965, Ap. J. 141, 811.

9. Kunze, H. J., 1968, "Plasma-Diagnostics," ed. W. Lochte-Holtgreven, North Holland, Amersterdam (Chapter 9).

10. Ali, A. and Griem, H., 1965, Phys. Rev. 140, 1044; 144, 336.

11. Sando, K., Doyle, R. and Dalgarno, A., 1969, Ap. J. 157, L 143.

12. Hammond, G., 1969, NOLTR, in preparation.

13. Hattenburg, A. T., 1967, Appl. Optics 6, 95.

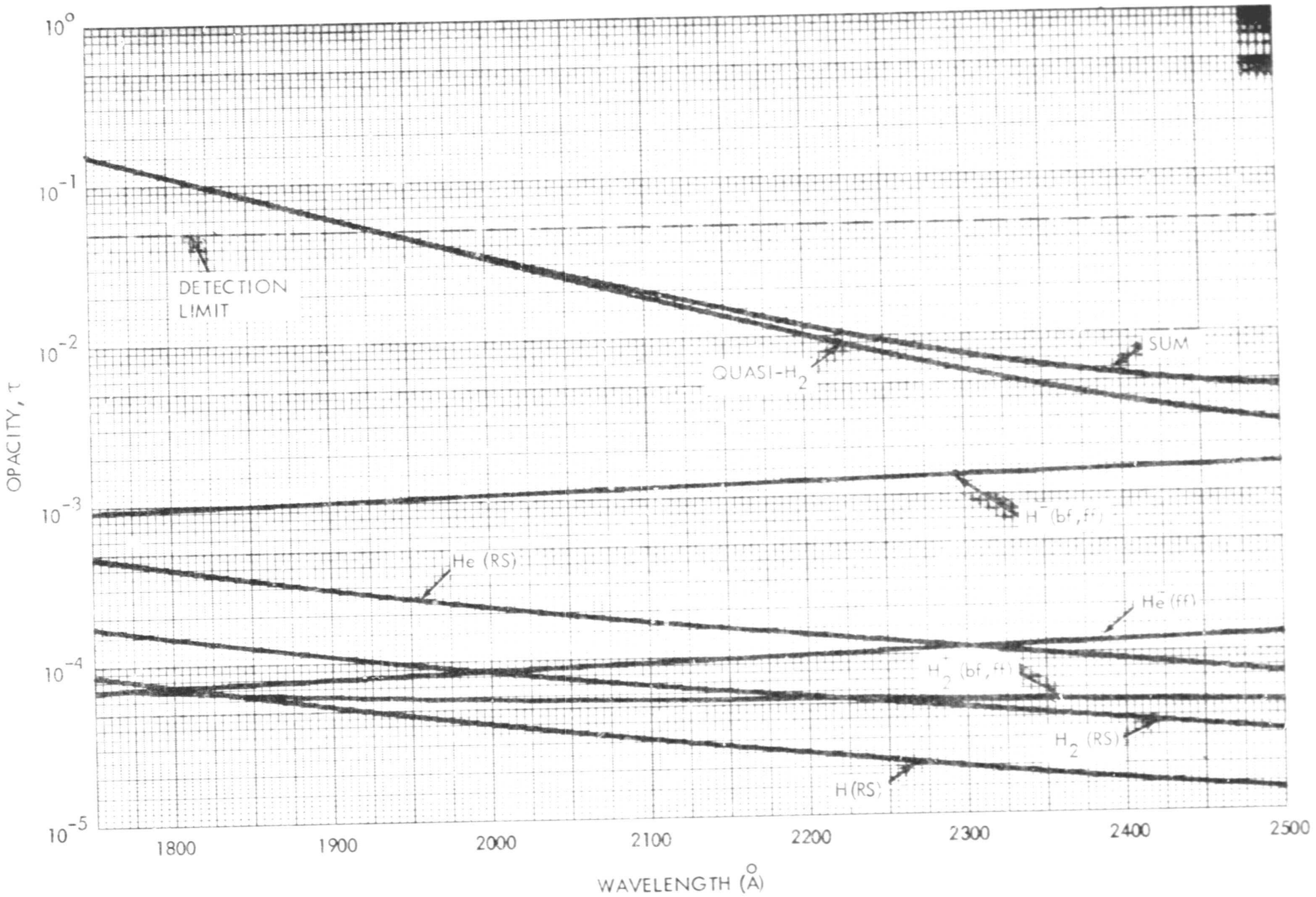

FIG. 1 CALCULATED OPACITY OF A 10% H_2/90% He MIXTURE FOR P= 2000 ATM., AND T = 5000°K.

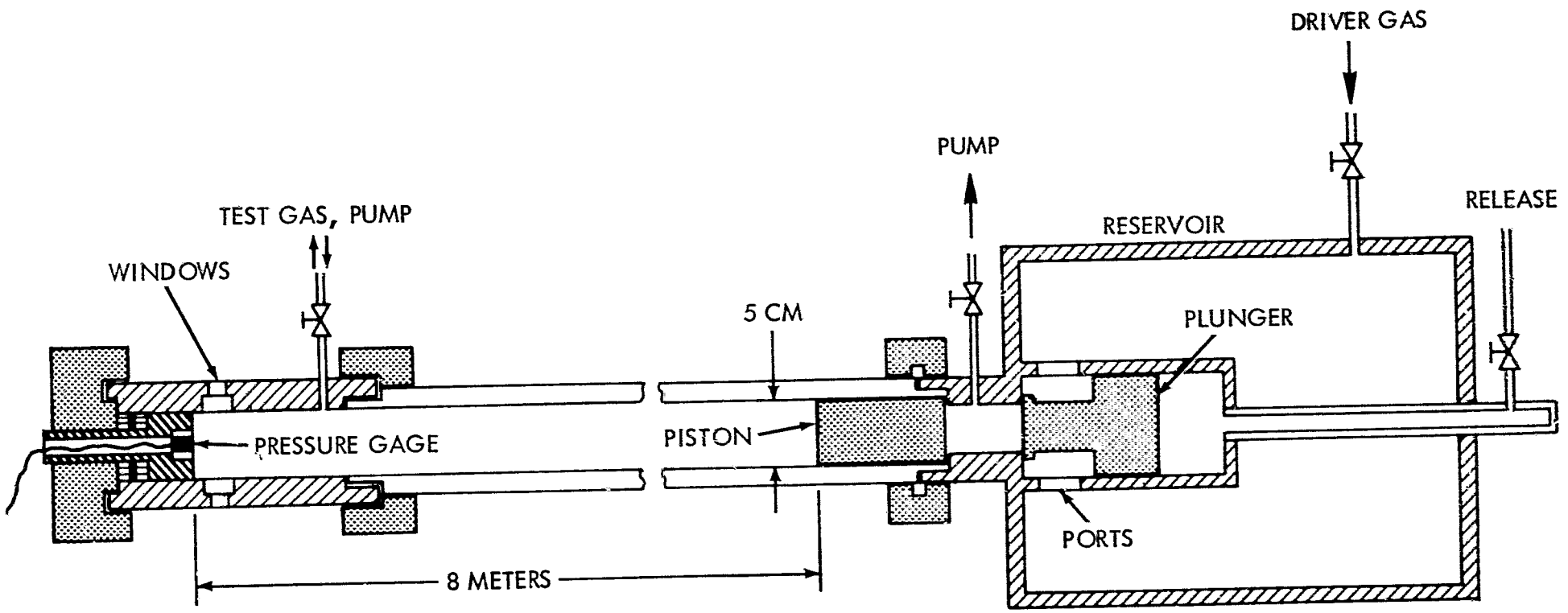

FIG. 2 . SCHEMATIC DIAGRAM OF BALLISTIC PISTON COMPRESSOR

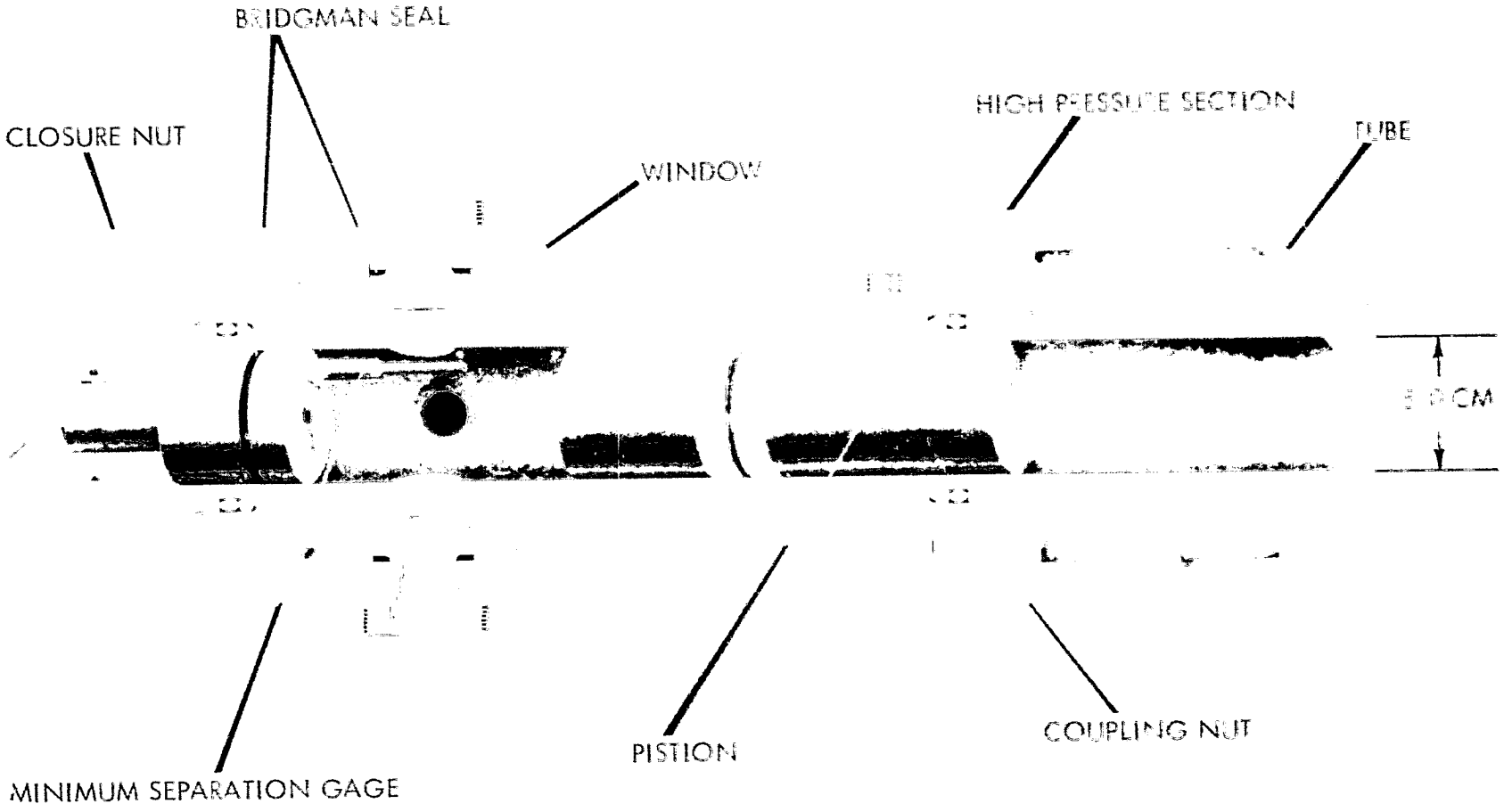

FIG. 3 HIGH PRESSURE TEST SECTION

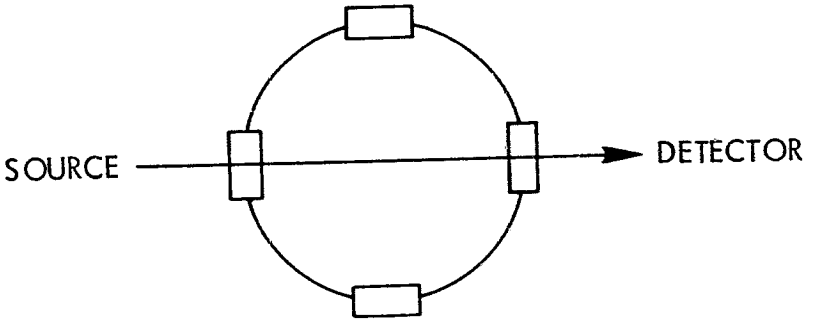

SINGLE PASS

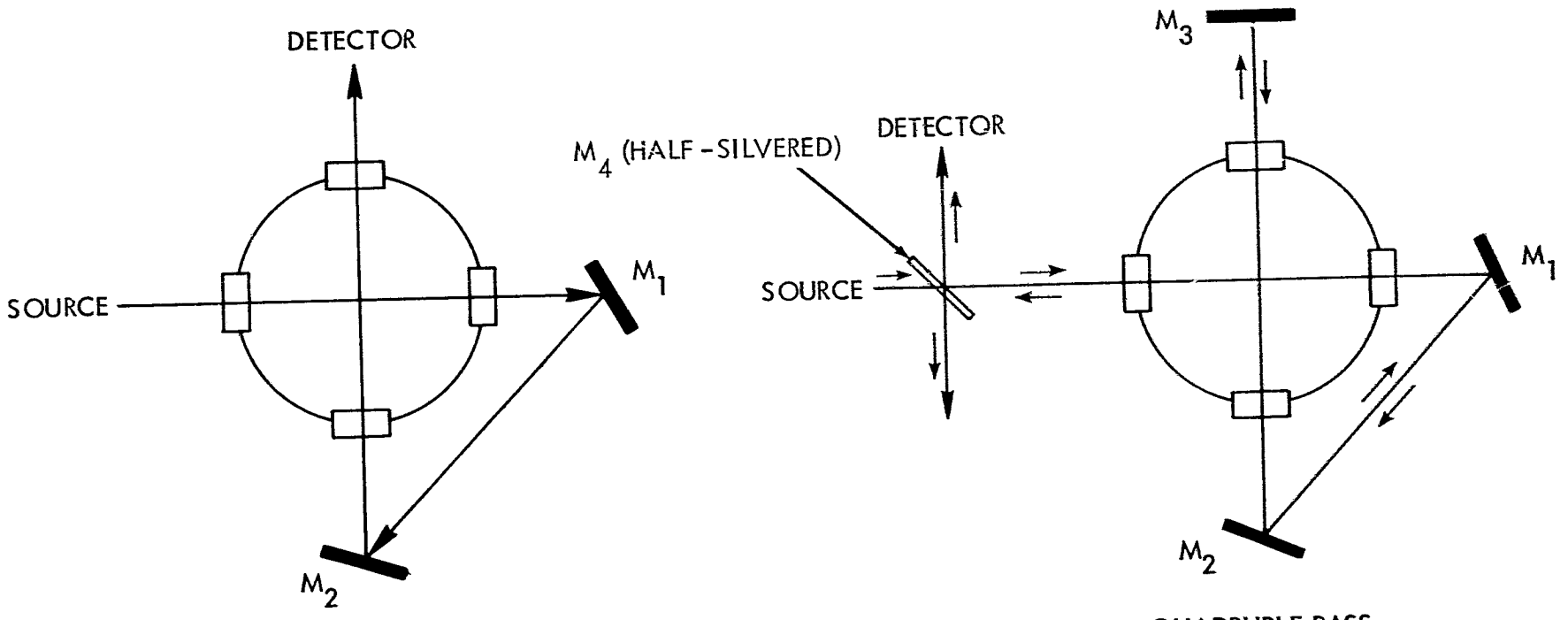

DOUBLE PASS

QUADRUPLE PASS

FIG. 4 MULTIPLE-PASS OPTICS FOR INCREASED DETECTION SENSITIVITY.

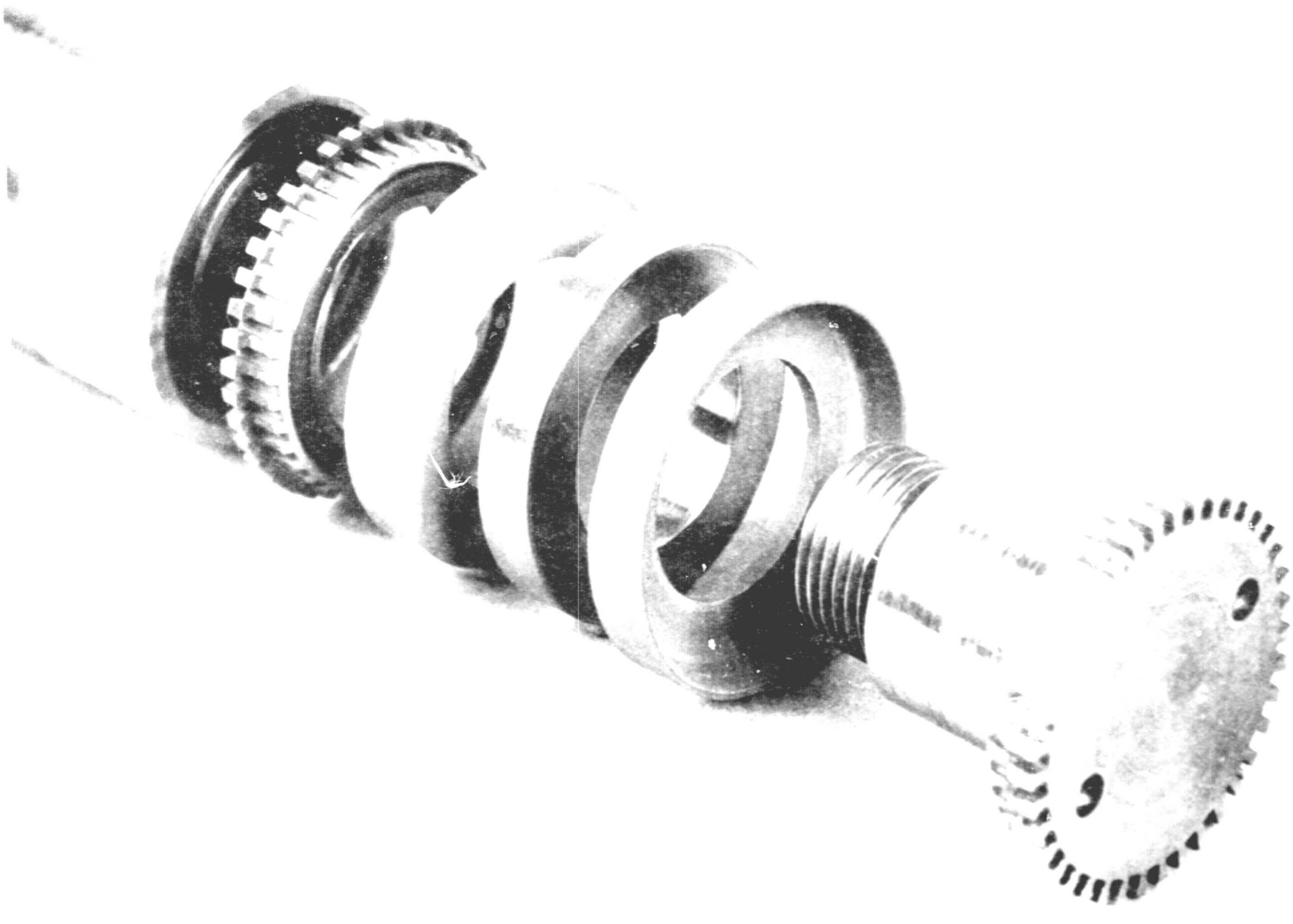

FIG. [illegible] UNASSEMBLED [illegible] DOUBLE-CUP PISTON SEAL

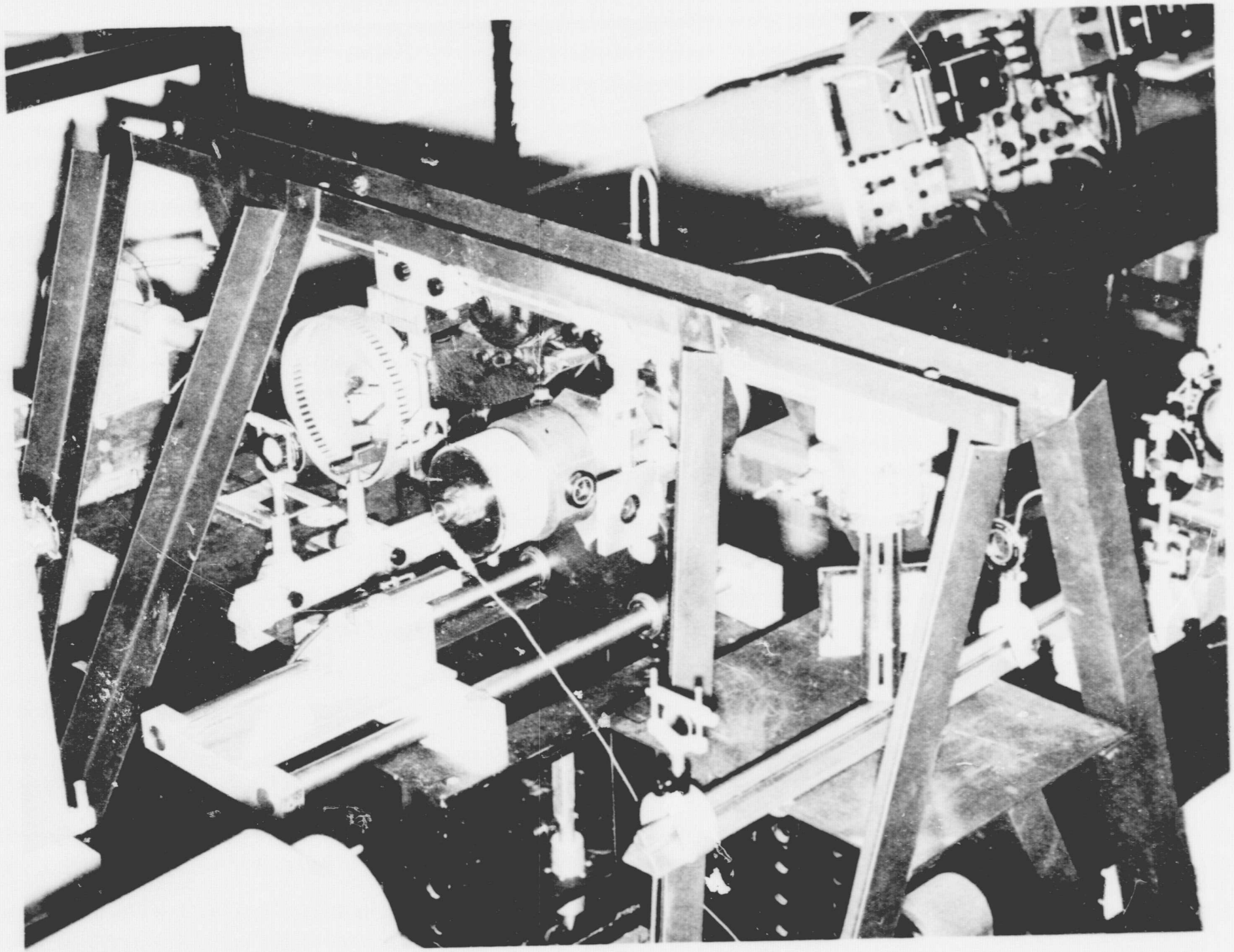

FIG. 6 OPTICAL BENCH ISOLATED FROM COMPRESSOR

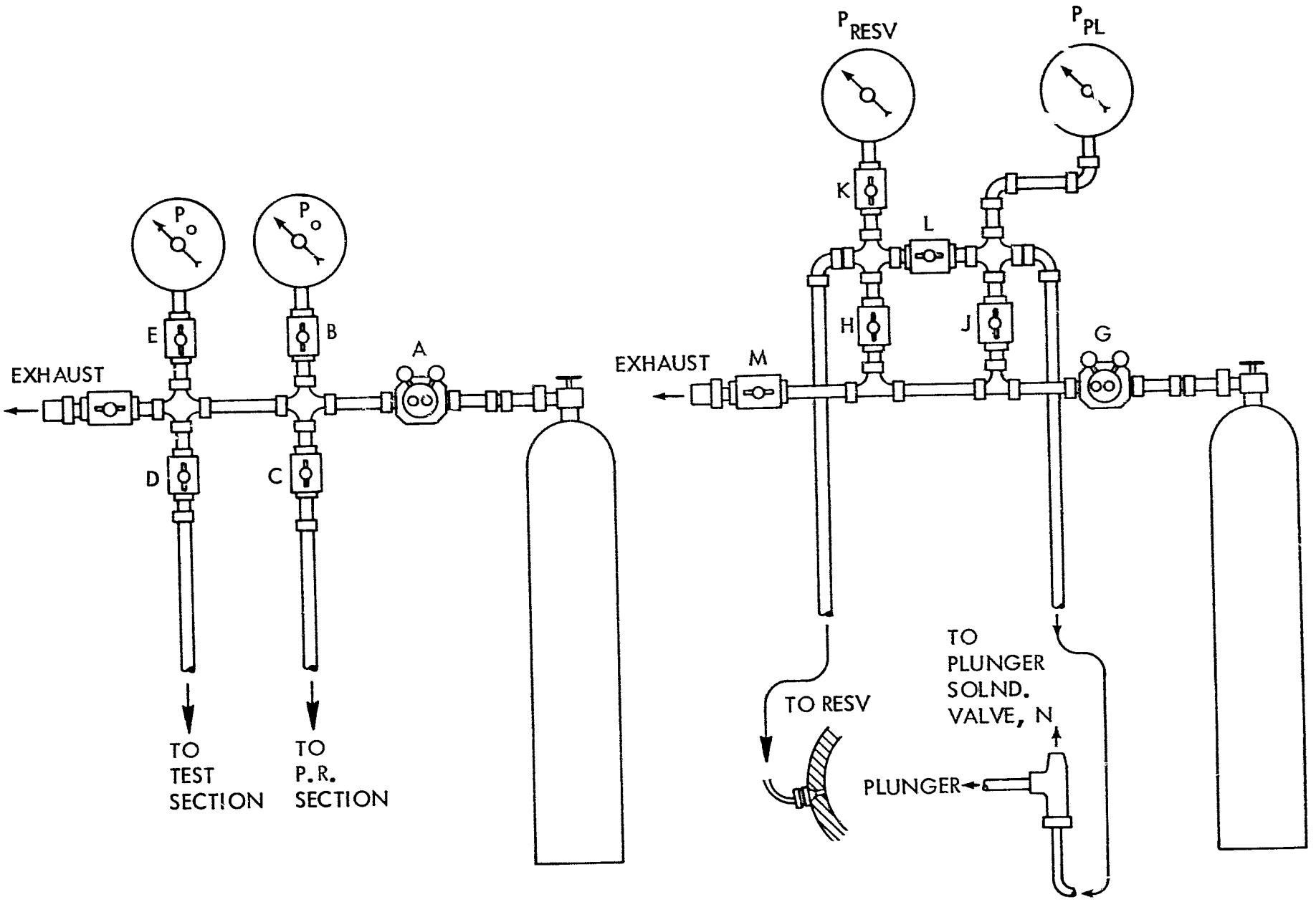

FIG. 7 REGULAR GAS-HANDLING SYSTEM

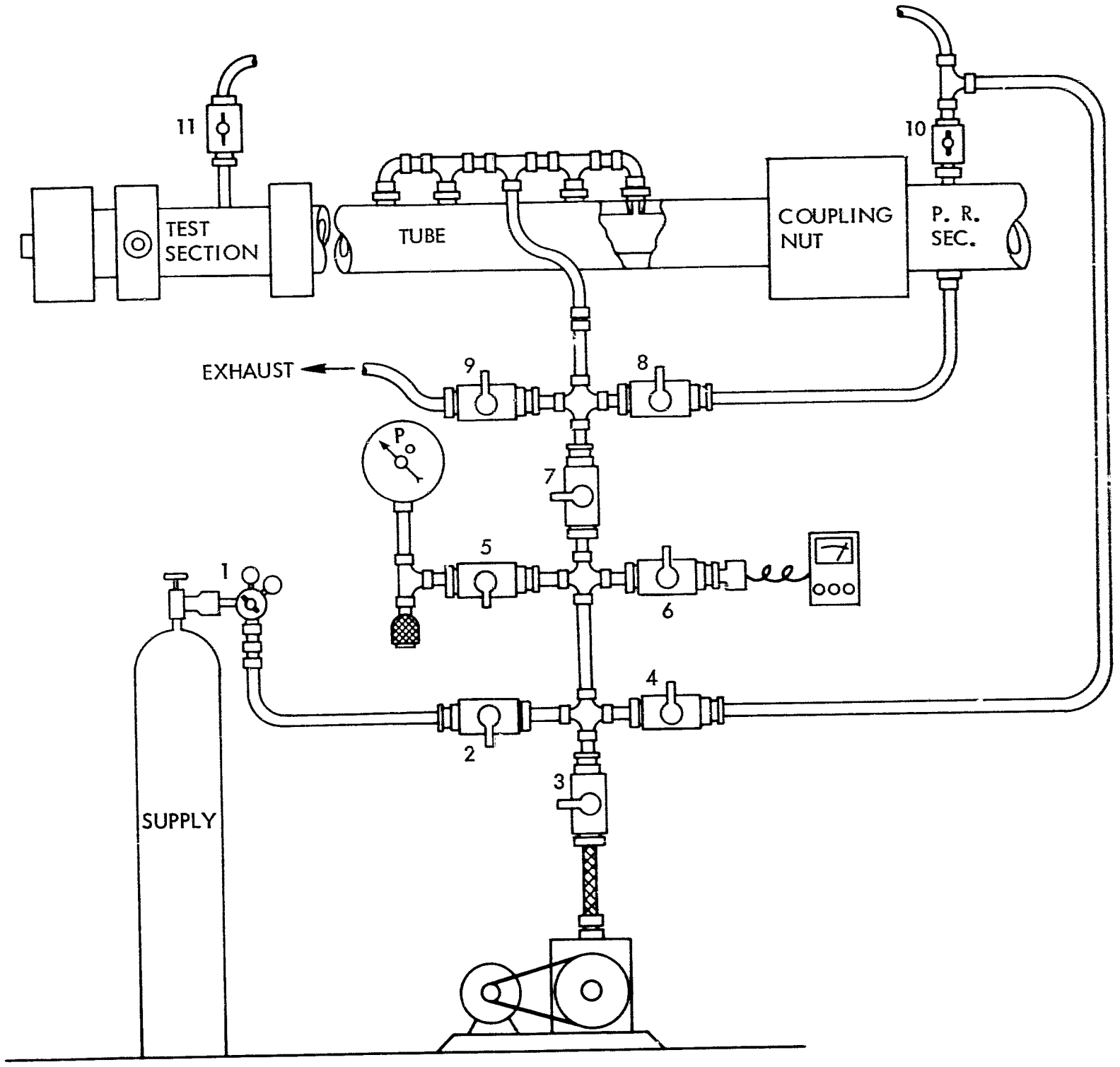

FIG. 8 HIGH PURITY GAS-HANDLING SYSTEM

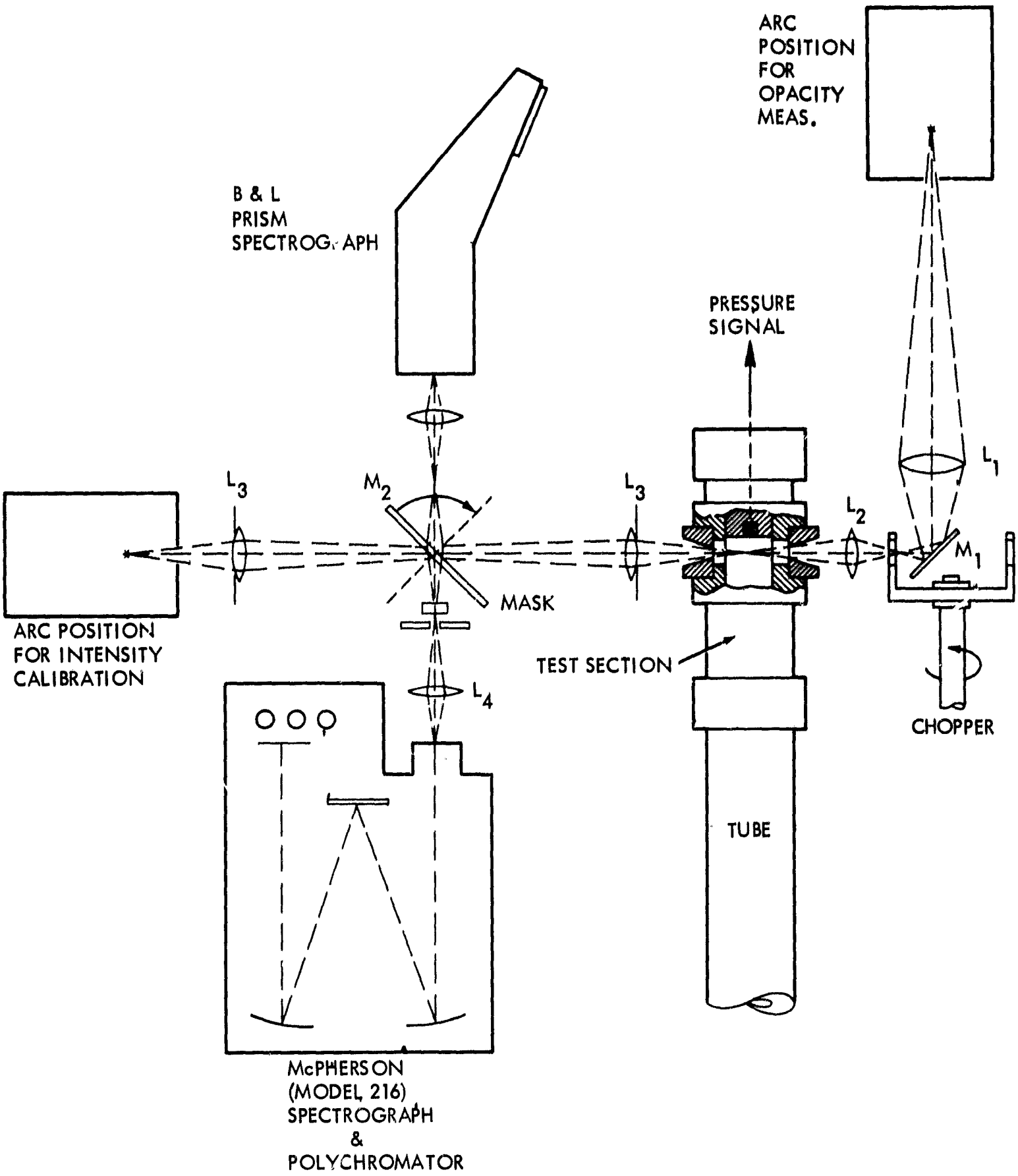

FIG. 9 OPTICS FOR TEMPERATURE MEASUREMENTS

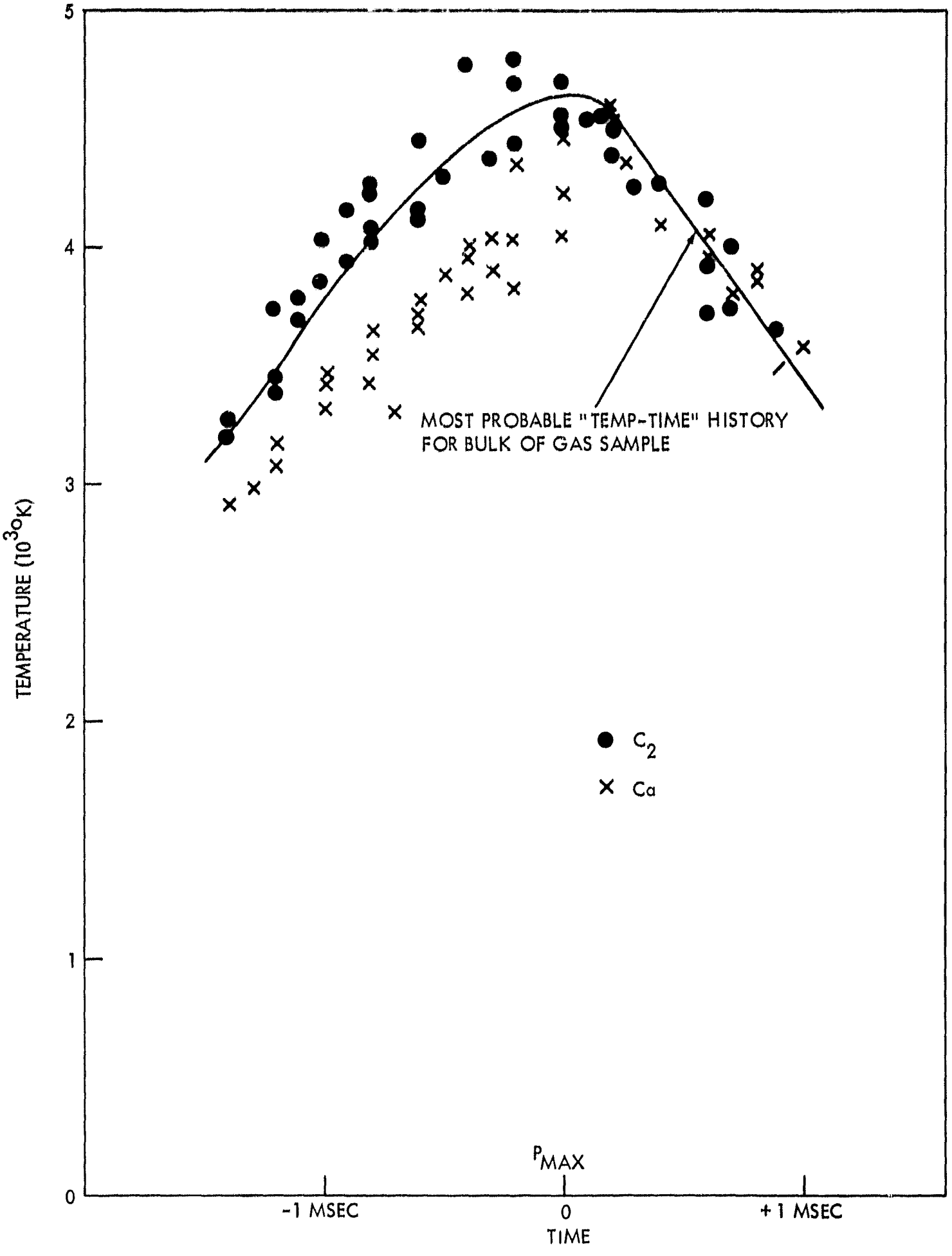

FIG. 10 SPECTROSCOPICALLY MEASURED TEMPERATURE FOR HELIUM.
THERMOMETRIC SPECIES: C_2, Ca

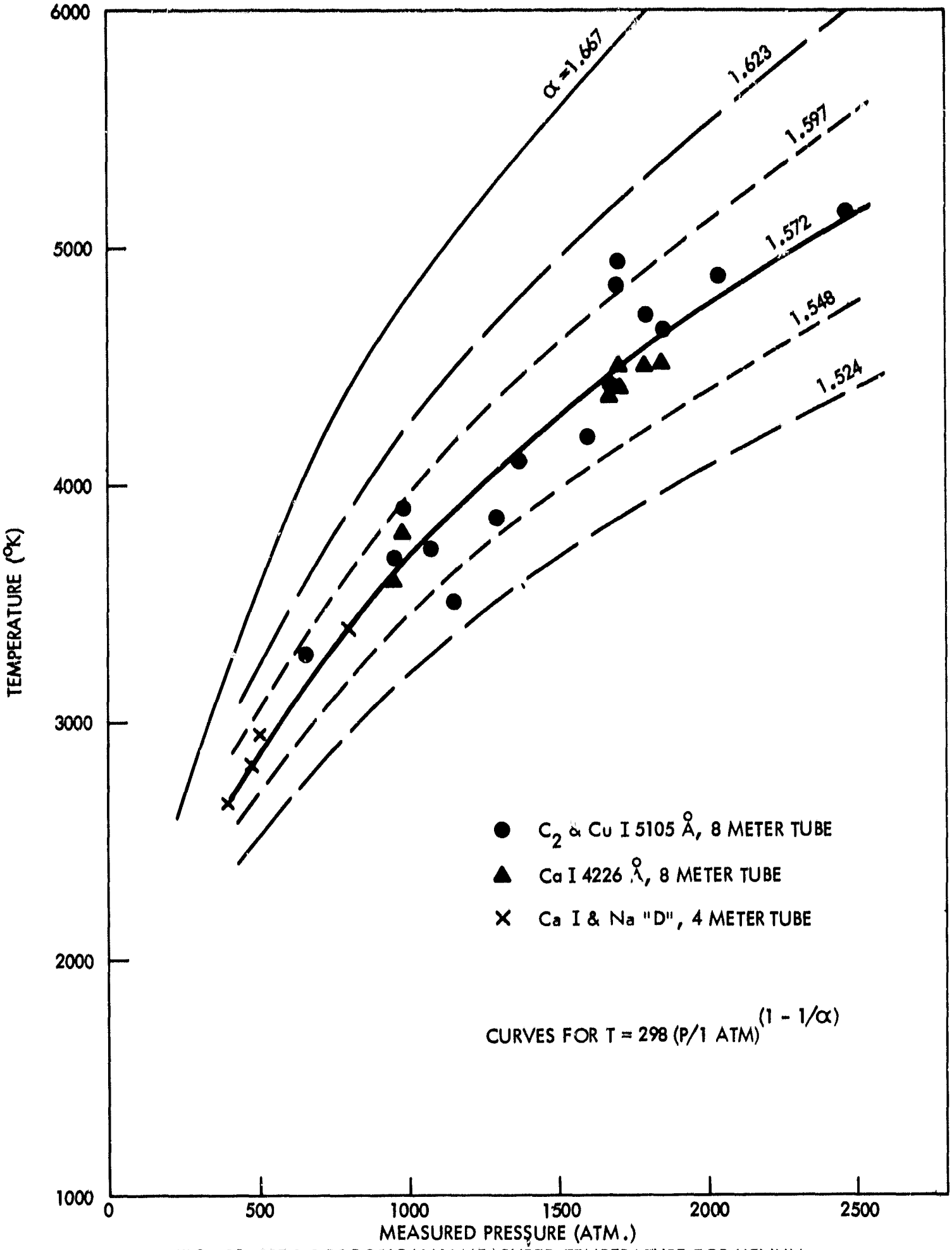

FIG. 11 SPECTROSCOPICALLY MEASURED TEMPERATURE FOR HELIUM.
THERMOMETRIC SPECIES: C_2, Ca, Cu, Na.

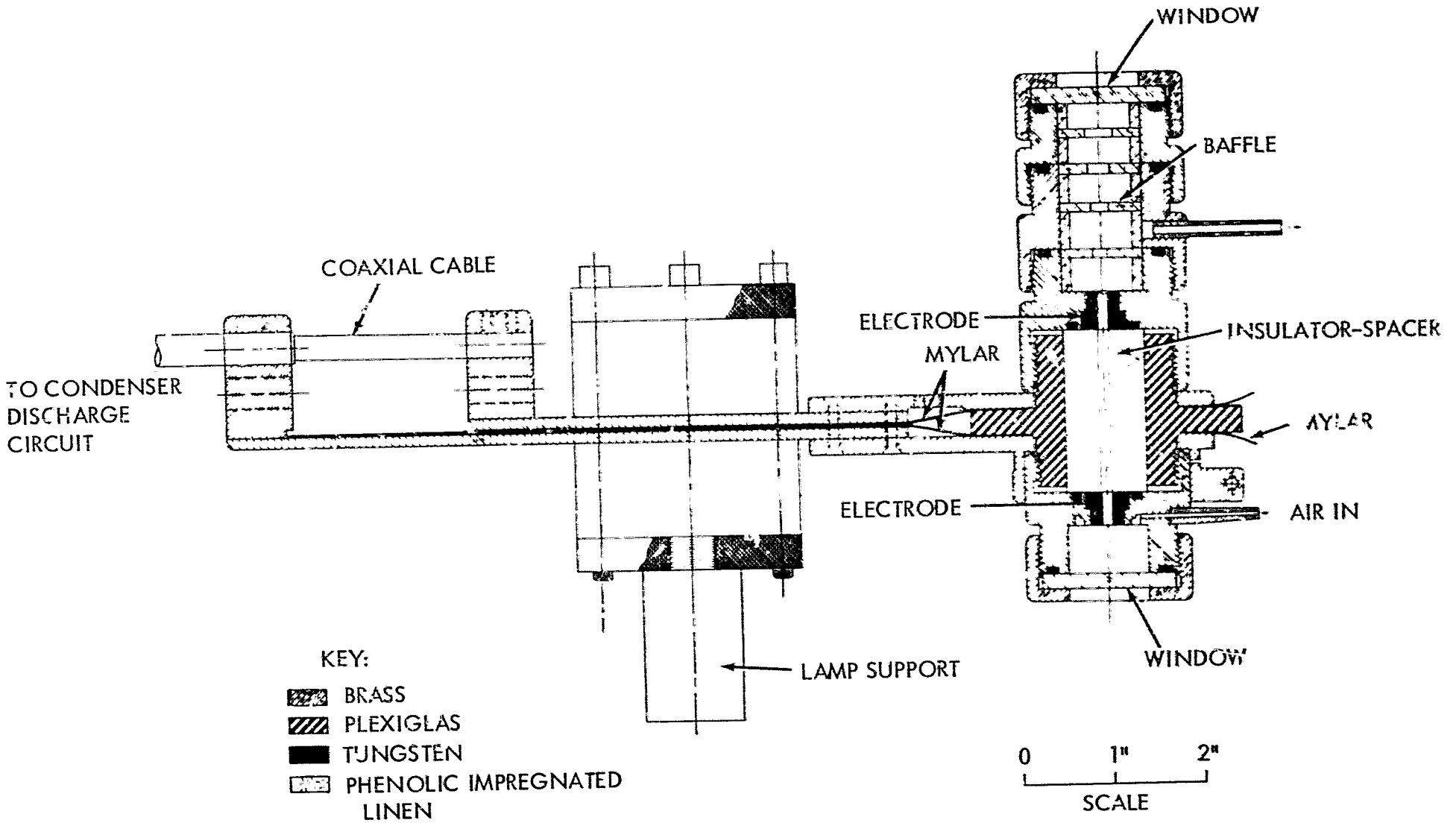

FIG. 12 HALF-SECTION OF FLASH LAMP ASSEMBLY

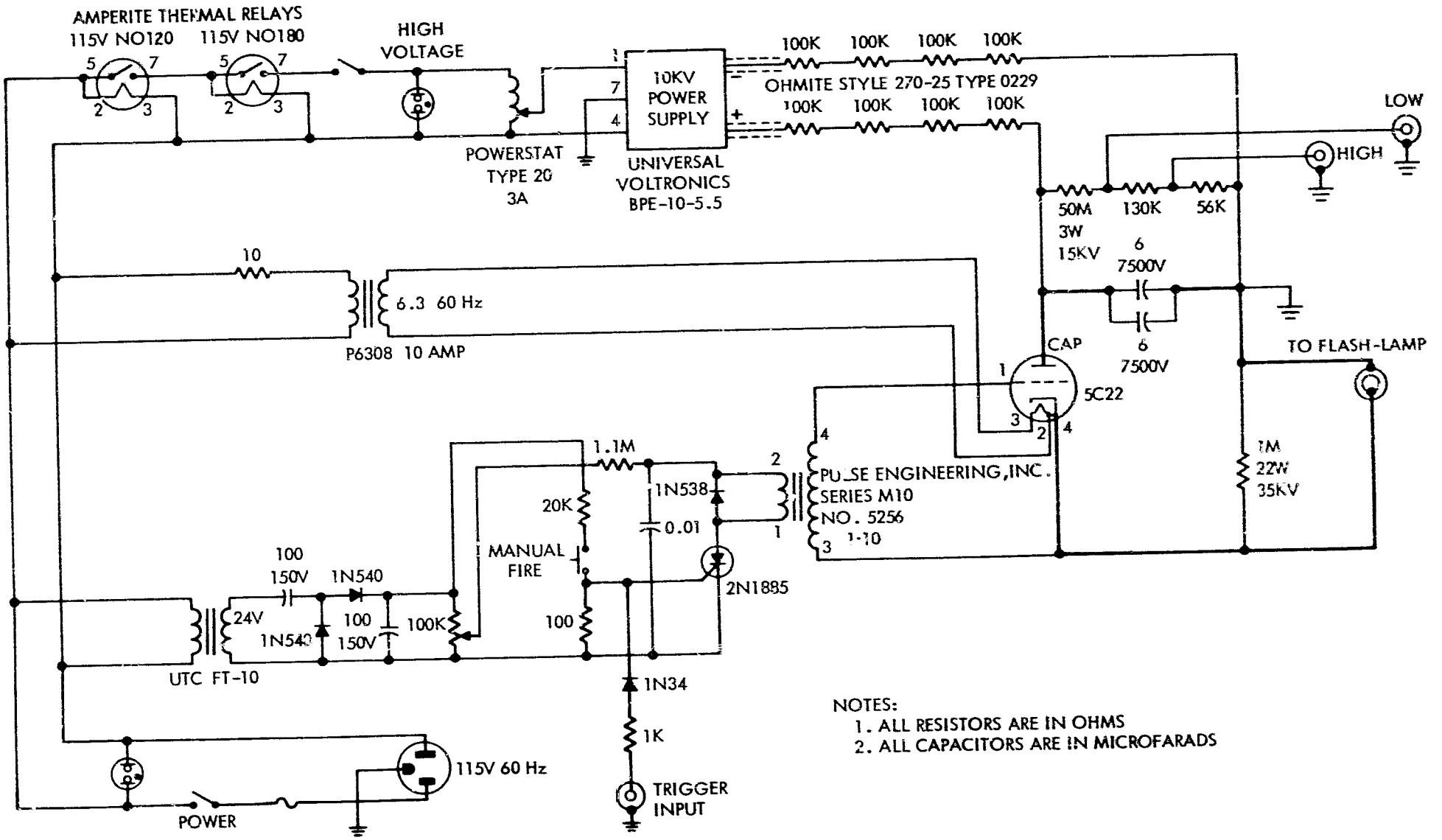

NOTES:
1. ALL RESISTORS ARE IN OHMS
2. ALL CAPACITORS ARE IN MICROFARADS

FIG. 13 FLASHLAMP CAPACITOR DISCHARGE CIRCUIT

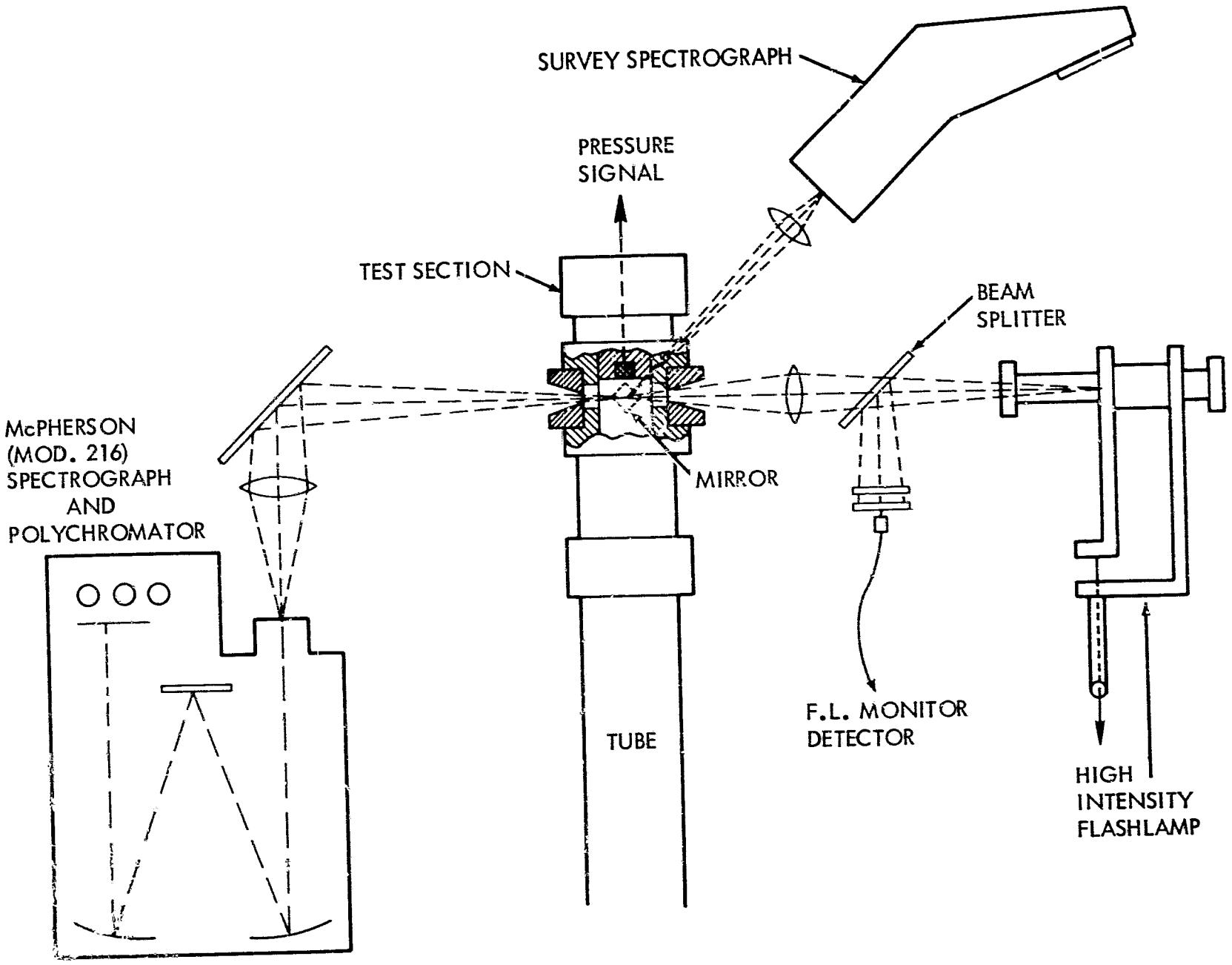

FIG. 14 OPTICS FOR ULTRAVIOLET OPACITY MEASUREMENTS

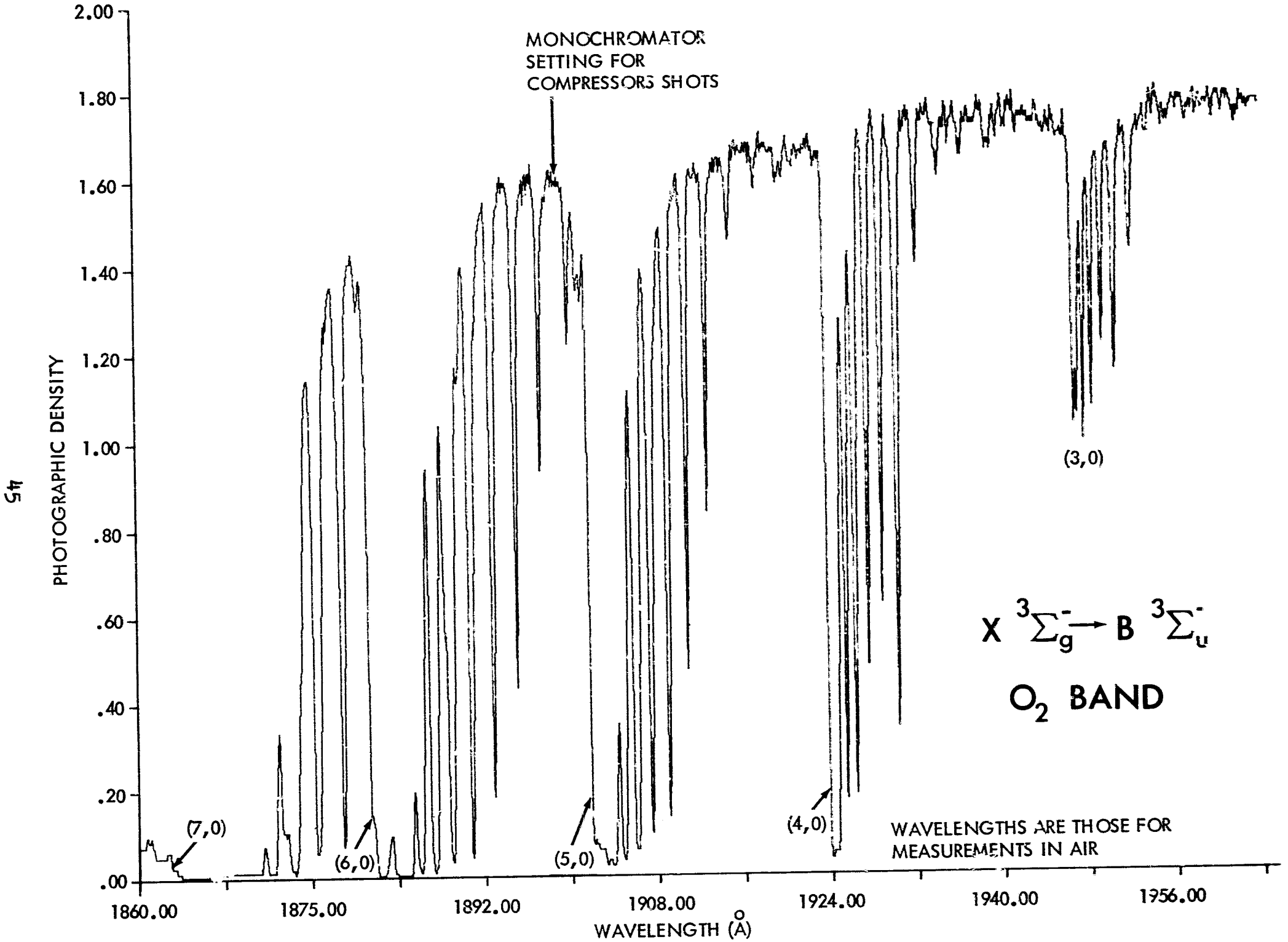

FIG. 15 FLASHLAMP AIR ABSORPTION SPECTRUM SHOWING ABSENCE OF SCATTERED LIGHT IN ULTRAVIOLET

DISTRIBUTION

	Copies
NASA-Lewis Research Center 21000 Brookpark Road Cleveland, Ohio 44135 Attn: Dr. R. W. Patch (106-1)	5
NASA-Lewis Research Center 21000 Brookpark Road Cleveland, Ohio 44135 Attn: Mr. Herman Barnett (500-309)	1
NASA-Lewis Research Center 21000 Brookpark Road Cleveland, Ohio 44135 Attn: Dr. B. Lubarsky (3-3)	1
NASA-Scientific and Technical Information Facility Box 33 College Park, Maryland Attn: NASA Representative	1
NASA-Lewis Research Center 21000 Brookpark Road Cleveland, Ohio 44135 Attn: Library (60-3)	1
NASA-Lewis Research Center 21000 Brookpark Road Cleveland, Ohio 44135 Attn: Dr. J. C. Liwosz (49-2)	1
NASA-Lewis Research Center 21000 Brookpark Road Cleveland, Ohio 44135 Attn: Technology Utilization Office (3-19)	1
NASA-Lewis Research Center 21000 Brookpark Road Cleveland, Ohio 44135 Attn: Mr. V. Hlavin (3-14)	1
Library Dept. of Physics and Astronomy University of Maryland College Park, Maryland 20740	1
Professor H. Griem Dept. of Physics and Astronomy University of Maryland College Park, Maryland 20740	1

DISTRIBUTION (Cont'd)

	Copies
Professor S. Y. Ch'en Physics Department University of Oregon Eugene, Oregon 97403	2
Professor M. Takeo Physics Department Portland State College Portland, Oregon	1
Dr. D. R. Stephens Lawrence Radiation Laboratory P. O Box 808 Livermore, California 94550	1
Dr. L. Merrill Assistant Director High Pressure Data Center P. O. Box 60, University Station Provo, Utah 84601	1
Dr. Raymond Moreau Baker Laboratory Cornell University Ithica, New York	1
Dr. William Condell ONR, Physics Program Code 421 Washington, D. C. 20360	1
Defense Documentation Center Cameron Station Alexandria, Virginia 22314	20